Journal of Advanced Research xxx (xxxx) xxx

Contents lists available at ScienceDirect

Journal of Advanced Research

journal homepage: www.elsevier.com/locate/jare

# Natural small molecule hinokitone mitigates NASH fibrosis by targeting regulation of FXR-mediated hepatocyte apoptosis

Ze-Jiang Ma [a,b,c,d], Ying-Kun Qiu [e], Zhe-Wei Yu [a,e], Tian-Tian Song [a,b,c], Yi-Tong Hu [a,b,c], An-Kang Peng [a,b,c,f], Rong Qi [a,b,c,*]

[a] Department of Pharmacology, School of Basic Medical Sciences, Peking University Health Science Center, 38 Xueyuan Road, Haidian District, Beijing 100191, China
[b] State Key Laboratory of Vascular Homeostasis and Remodeling, State Key Laboratory of Natural and Biomimetic Drugs, NHC Key Laboratory of Cardiovascular Molecular Biology and Regulatory Peptides, Peking University, Beijing 100191, China
[c] Beijing Key Laboratory of Molecular Pharmaceutics and New Drug Delivery Systems, Beijing 100191, China
[d] Department of Physiology, School of Basic Medical Sciences, Xinjiang Second Medical College, Karamay, China
[e] Fujian Provincial Key Laboratory of Innovative Drug Target Research, School of Pharmaceutical Sciences, Xiamen University, Xiamen, China
[f] Department of Cardiology, Pu'er People's Hospital, Yunnan, China

## HIGHLIGHTS

- Natural small molecule HO inhibits liver fibrosis in a mouse NASH model.
- Hepatocyte FXR mediates the effect of HO anti-liver fibrosis.
- HO bindis to and upregulates the protein level of FXR, which exerting an anti-apoptotic effect on hepatocytes.
- HO indirectly preventing HSCs activation through inhibiting hepatocyte apoptosis.

## GRAPHICAL ABSTRACT

Hinokitone exerts an inhibitory effect on NASH fibrosis. Mechanistically, Hinokitone attenuates hepatocyte apoptosis by targeting the upregulation of hepatocyte FXR, which in turn indirectly inhibits HSC activation.

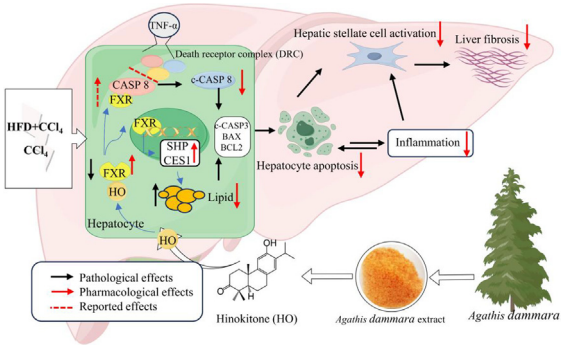


## ARTICLE INFO

*Article history:*
Received 21 July 2024
Revised 23 September 2024
Accepted 10 December 2024
Available online xxxx

## ABSTRACT

*Introduction:* Liver fibrosis is the common fate of NASH and poses a major health threat with very limited pharmacological treatments.
*Objectives:* This study aims to investigate the preventive effect of hinokitone (HO), an isolated compound from *Agathis dammara*, on NASH fibrosis and its underlying mechanism.

*Abbreviations:* α-SMA, alpha smooth muscle actin; AST, aspartate transaminase; ALT, aspartate aminotransferase; Act-D, Actinomycin-D; BAX, BcL2-Associated X; BCL2, B-cell lymphoma-2; CASP3, cysteinyl aspartate specific proteinase 3; c-CASP3, cleaved cysteinyl aspartate specific proteinase 3; CASP 8, cysteinyl aspartate specific proteinase 8; c-CASP 8, cleaved cysteinyl aspartate specific proteinase 8; COL1, collagen Type I; COL3, collagen Type III; CD, chow diet; CES1, Carboxylesterases 1; CHX, cycloheximide; FASN, fatty acid synthase; FXR, farnesoid X receptor; GAPDH, glyceraldehyde-3-phosphate dehydrogenase; H&E, hematoxylin and eosin; HFD, high fat diet; HO, hinokitone; HSCs, Hepatic stellate cells; IP, Intraperitoneal injection; KO, Knockout; LXR, liver X receptor; NAFLD, nonalcoholic fatty liver disease; NASH, nonalcoholic steatohepatitis; PA, palmitic acid; SHP, small heterodimer partner; SREBP1c, sterol regulatory element-binding protein-1c; TGF-β, transforming growth factor β; TNFα, tumor necrosis factor α; RNA, ribonucleic acid; TG, triglyceride; WT, Wide type.

* Corresponding author.
*E-mail address:* ronaqi@bjmu.edu.cn (R. Qi).

https://doi.org/10.1016/j.jare.2024.12.016


Please cite this article as: Z.-J. Ma, Y.-K. Qiu, Z.-W. Yu et al., Natural small molecule hinokitone mitigates NASH fibrosis by targeting regulation of FXR-mediated hepatocyte apoptosis, Journal of Advanced Research, https://doi.org/10.1016/j.jare.2024.12.016

*Keywords:*
Hinokitone
Non-alcoholic steatohepatitis
Liver fibrosis
Farnesoid X receptor
Hepatocyte apoptosis

*Methods:* To investigate the effect of HO on NASH fibrosis, C57BL/6 mice were either fed a high-fat diet (HFD) in conjunction with intraperitoneal injection of $CCl_4$ for 8 weeks or single $CCl_4$ for 14 days to establish mouse liver fibrosis model, and HO was administered by gavage simultaneously. To elucidate the underlying mechanisms, HepG2 cells were stimulated by palmitic acid (PA) or tumor necrosis factor α plus actinomycin-D (Act-D + TNFα) to induce hepatocyte apoptosis model. Furthermore, hepatocyte Farnesoid-X-receptor (FXR) specifically knocked out mice were established by the albumin-Cre-loxP recombination enzyme system to ascertain the role of FXR in the anti-NASH fibrosis effects of HO.
*Results:* The results showed that HO presented dose-dependent anti-liver fibrosis efficacy in NASH mice induced by HFD + $CCl_4$ and $CCl_4$-induced mouse liver fibrosis. Cellularly, HO significantly inhibited PA-induced lipotoxic apoptosis and Act-D + TNFα-induced exogenous apoptosis in hepatocytes, which in turn prevented HSC activation. Mechanistically, bioinformatics analysis and surface plasmon resonance assay had identified hepatocyte FXR as a target of HO. Specifically, HO directly bound to FXR and upregulated its protein level by inhibiting proteasomal degradation. In turn, HO attenuated hepatocyte lipid deposition through upregulating the FXR's downstream target genes *SHP* and *CES1*, and reduced cleaved-CASP8 level, thereby inhibiting hepatocyte apoptosis. Furthermore, HO lost its function in the inhibition of hepatocyte apoptosis and liver fibrosis when knockout hepatocyte FXR.
*Conclusion:* In conclusion, HO has an inhibitory effect on NASH fibrosis. This effect is mediated by targeting upregulation of hepatocyte FXR, which in turn attenuates hepatocyte apoptosis and thus indirectly inhibits the activation of HSCs.


## Introduction

Non-alcoholic fatty liver disease (NAFLD) has become the most common chronic liver disease with a global average prevalence of up to 30 %, representing a significant global public health burden [1,2]. Non-alcoholic steatohepatitis (NASH) is a progressive stage of NAFLD with steatosis, hepatocellular ballooning, periductal inflammation and varying degrees of fibrosis[3]. Among the histological features of NASH, the severity of fibrosis is predictive of long-term outcomes in patients with NASH and is strongly associated with liver-related mortality[4,5]. Although activated hepatic stellate cells (HSCs) have been shown to be the primary cells for collagen production, the progression of fibrosis in NASH results from a combination of interactions including hepatocyte lipotoxic injury, apoptosis and other non-parenchymal cellular interactions and influences[6,7]. Hepatocyte apoptosis, as a central event, directly or indirectly causes HSCs activation through the apoptotic body, damage-associated molecular pattern and intercellular communication, which in turn leads to fibrosis and exacerbates the progression of NASH toward cirrhosis or even hepatocellular carcinoma [8,9]. However, there is only one drug, Rezdiffra, that has been approved recently by the US FDA for treatment of NASH fibrosis. Investigation and development of anti-NASH fibrosis drugs to meet the needs of disease prevention and treatment are still in demand.

Farnesoid X receptor (FXR), a nuclear receptor activated by bile acid and highly expressed in hepatocytes. It is capable of regulating gene transcription and expression by binding to various FXR-responsive elements on downstream target genes, either as a monomer, homodimer, or heterodimer with the retinoid X receptor. Which can regulate the expression of genes related to lipid metabolism (SREBP1c), bile acid metabolism (cholesterol 7α hydroxylase), and glucose metabolism (phosphoenolpyruvate carboxykinase, glucose 6-phosphate) through its direct target gene small heterodimer partner (SHP). For which, it has been demonstrated that FXR represents a reliable target for the intervention of disease in NASH[10]. In addition, Carboxylesterases 1 (CES1) is also highly expressed in hepatocytes and is a principal enzyme for lipid hydrolysis, as well as a pivotal regulator in the pathogenesis of NASH. The study by Xu, J et al. found that the promoter sequence of CES1 contains an FXR response binding element (FXRE), FXR regulates the expression level of CES1 through the FXRE and that CES1 partially mediates the function of FXR to inhibit lipid deposition and protect hepatocytes [11]. Furthermore, recent studies have demonstrated that FXR proteins are capable of binding to cysteinyl aspartate specific proteinase 8 (CASP8) in the cytoplasm through a non-classical function, preventing the assembly of death receptor complexes, inhibiting CASP8 cleaving and suppressing hepatocyte apoptosis, thereby exerting an anti-liver fibrosis effect [12]. Therefore, FXR exerts its protective effects on the liver through two distinct mechanisms. Firstly, it improves lipid metabolism through its transcriptional regulation function, thereby inhibiting the development of NASH fibrosis. Secondly, FXR inhibits the progression of liver fibrosis by directly regulating hepatocyte apoptosis, thereby sparing HSCs from activation.

*Agathis dammara* (Lamb.) Rich is a tree belonging to the genus Agathis, native to the Philippines and the Malay Peninsula. It is used in Malaysia to treat a range of common ailments, including stomachache, constipation and arthritis [13]. Furthermore, the biological constituents presented in *Agathis dammara* have been documented to exert hypoglycemic, hypolipidemic, anti-inflammatory, antioxidant and anti-melanogenic effects [14]. Our previous work has demonstrated that *Agathis dammara* extract obtained from the heartwood of *Agathis dammara* and hinokitone (HO, an isolated monomer from *Agathis dammara*) can inhibit lipid deposition induced by oleic acid in HepG2 hepatocytes [15,16]. These findings indicate that HO may possess the capacity to regulate lipid metabolism. However, it has remained to be clarified whether HO has an inhibitory effect on NASH fibrosis. In light of the promotion and exacerbation of hepatocyte lipotoxic injury and apoptosis on the development of liver fibrosis, we hypothesize that HO might have efficacy in inhibiting the development of NASH fibrosis.

In the present study, we aimed to elucidate the role of HO in the inhibition of NASH fibrosis and to identify its mechanism of action and key targets, with a view to providing a new effective strategy for the treatment of NASH fibrosis.

## Materials and methods

### Cell culture

LX2 cells (purchased from Zhejiang Meisen Cell Technology Co., Ltd.) and HepG2 cells (purchased from Dalian Meilun Biotechnology Co., Ltd.) were cultured in DEMEM medium containing 10 % fetal bovine serum and 1 % penicillin–streptomycin double

antibiotic at 37 °C under 5 % CO2. Primary hepatocytes were extracted from wild type mice ($FXR^{WT}$) and FXR hepatocyte-specific knockout ($FXR^{KO}$) mice and cultured under the same conditions as above. A model of hepatic stellate cell activation was established by treating LX2 cells with 10 ng/mL of TGF-β, which named TGF-β group. 200 μmol/L palmitic acid was used to treat HepG2 cells or primary hepatocytes for 24 h to establish a lipotoxic apoptosis model, named PA group. And 20 ng/mL TNFα combined with 0.2 μmol/L Act-D were treat HepG2 cells or primary hepatocytes to establish a l lipotoxic apoptosis model, named Act-D + TNFα group. The apoptosis model of receptor signaling was established with 0.2 μmol/L Act-D for 12 h. 10/20 μmol/L of HO was given while modeling. The hepatocyte-hepatic stellate cell interaction model was constructed according to the method of Hong et al[12]. The conditioned medium of apoptotic hepatocytes established as above combined with 5 ng/mL of TGF-β was used to treat the LX2 cells for 24 h, and the hepatocyte-hepatic stellate cell interaction was evaluated. HepG2 cells were inoculated into 12-well plates, and 20 μmol/L actinomycin ketone (CHX) was added at a final concentration of 20 μmol/L for 2 h, 4 h, 6 h, 8 h and 12 h to inhibit protein synthesis, and 20 μmol/L HO was added at a final concentration of 20 μmol/L to pretreat for 12 h, which was used for the FXR protein degradation assay. Once the experimental period had concluded, the cells were harvested for subsequent analysis.

*Annexin V-FITC/PI apoptosis assay*

After treating the HepG2 cells with PA and HO, the cell samples were washed twice with PBS, centrifuged at 1000 × g for 5 min, and resuspended in a cold D-Hanks buffer to a concentration of $1 \times 10^6$ cells/mL. Subsequently, 10 μL of Annexin V-FITC and 10 μL of propidium iodide (PI) were added to 100 μL of the cell suspension, followed by incubation for 15 min at room temperature in the dark. The AnnexinV-FITC probe binds to phosphatidylserine flipped from the inner surface of the cell membrane to the outer surface of the cell membrane, and propidium iodide passes through the damaged cell membrane and binds to the DNA, displaying fluorescence upon different laser excitations, thus distinguishing between living, early apoptotic and necrotic cells. Finally, flow cytometry (FCM) analysis was performed to evaluate the effects of HO on PA-induced apoptosis of hepatocytes.

*Animals for in vivo studies*

Male C57BL/6 mice, aged 8–10 weeks and weighing approximately 20–25 g, were used in the study and purchased from the Animal Department of Peking University Health Science Center. Mice with flox loci on both alleles of FXR ($FXR^{flox/flox}$) mice were provided by Prof. Chang-Tao Jiang at Peking University, and hepatocyte-specific albumin (ALB)-mediated cyclisation recombination enzyme (Cre)-transgenic mice were from Prof. Yong-Sheng Chang at Tianjin Medical University. Hepatocyte FXR was specifically knocked out by hybridization using the Cre-loxP recombination enzyme system, and hepatocyte FXR-specific knockout mice ($FXR^{floxp/floxp}$, ALB-Cre, $FXR^{KO}$) were obtained in addition to mice identified as non-Cre-expressing as littermate controls ($FXR^{flox/flox}$, $FXR^{WT}$). The primer sequences used for genotyping are shown in Table 1. Mice were kept under a 12-hour light/dark cycle and had free access to food and water. The ambient temperature and humidity were maintained at 25 ± 2°C and 50 %, respectively. The breeding and application of animals in experiments adhere to the National Institutes of Health Guidelines for the Application of Laboratory Animals. All animal experiments have been reviewed and approved by the Animal Ethics Committee of the Faculty of Medicine of Peking University (Approval No. LA2021045).

**Table 1**
Primer sequences used for genotyping.

| Gene | | Sequence |
|---|---|---|
| *Albumin-Cre* | Forward | GAA GCA GAA GCT TAG GAA GAT GG |
| *Albumin* | Forward | TGC AAA CAT CAC ATG CAC AC |
| *Common* | Reverse | TTG GCC CCT TAC CAT AAC TG |
| $FXR^{flox}$ | Reverse | ATA GAC AAC CCC AGT GAC CC |
| $FXR^{flox}$ | Forward | TCT AAA GGA TAG CCG AAT CT |

*Mouse NASH fibrosis co-induced by HFD and $CCl_4$ and HO treatment*

The male mice were randomly divided into three groups, with 5–8 mice in each group. For the control group, mice were fed a chow-diet, named CD group. For the model group, to induce NASH fibrosis, mice were fed a high-fat diet (HFD) and intraperitoneally injected with 20 % $CCl_4$ ($CCl_4$ dissolved in olive oil, V/V = 1:9, injected 4 mL/kg body weight) twice a week for a duration of 8 weeks[17], named HFD + $CCl_4$ group. HO-treated mice received 100/33/11 mg/kg/day HO (dissolved in 0.5 % sodium carboxymethyl cellulose) by gavage from the start of HFD + $CCl_4$ treatment, named HFD + $CCl_4$ + HO-H, HFD + $CCl_4$ + HO-M, HFD + $CCl_4$ + HO-L, respectively. Mice in the CD group and HFD + $CCl_4$ group were treated with the vehicle (0.5 % sodium carboxymethyl cellulose). Body weights were recorded on a daily basis throughout the experimental period, and the mice were subsequently euthanised at the conclusion of the experiment via the administration of 0.8 % pentobarbital sodium anaesthesia, with blood collected from the inner canthus. The blood was spun at 3000 rpm for 15 min at room temperature, and the serum was stored at −80 °C. Once the livers of the mice had been perfused with PBS until they had turned completely white, the organs were excised, weighed, and then the tissues were divided. Some of the tissues were fixed in 4 % paraformaldehyde overnight and then stored in 20 % sucrose for staining of the tissue sections, while the remainder were stored in a refrigerator at −80 °C for the extraction of protein and total RNA.

*$CCl_4$-induced mouse liver fibrosis and HO treatment*

C57BL/6J male mice or littermate bred control wild-type ($FXR^{WT}$) and hepatocyte FXR-specific knockout ($FXR^{KO}$) mice were randomly allocated. The control group received olive oil (4 mL/kg) intraperitoneally three times a week and solvent (8 mL/kg) by gavage daily. The model group ($CCl_4$ group) and the drug administration group received $CCl_4$ ($CCl_4$: olive oil = 1:7, 4 mL/kg) by intraperitoneal injection three times a week, while the drug administration group received 100 mg/kg HO (dissolved in 0.5 % sodium carboxymethyl cellulose) by gavage daily, named $CCl_4$ + HO group. Mice in the control group and $CCl_4$ group were treated with the vehicle (0.5 % sodium carboxymethyl cellulose). At the conclusion of the experiment, the mice were treated in accordance with the aforementioned methodology.

*Hematoxylin-eosin (H&E) staining*

The liver slides were subjected to dewaxing by immersing them in xylene three times for 10 min each. Subsequently, they were washed with 100 %, 95 %, 80 %, and 70 % alcohol for 5 min each to remove the xylene. After rinsing with running water, the slides were stained with hematoxylin solution for 3 min and then dehydrated with 85 % and 95 % alcohol for 5 min each. Next, the slides were stained with eosin solution for 3 min. Finally, the slides were sequentially dehydrated with 70 %, 80 %, 95 %, and 100 % alcohol, followed by xylene, for 5 min each. They were then sealed with resin.

*Sirius Red staining*

The slides were dewaxed using the method mentioned above, and xylene was eliminated. Subsequently, the slides were stained with Sirius Red staining solution for 1 h. After staining, the slides

were rinsed under running water, dehydrated using a graded series of alcohol and xylene, and finally mounted with resin, following the same protocol as described above for H&E staining.

*Oil Red O staining*

The liver slides were fixed with 4 % paraformaldehyde for 10 min and subsequently washed with PBS three times. Then, the slides were immersed in 60 % isopropanol for 10 min, stained with Oil Red O for 30 min, and rinsed with 60 % isopropanol to remove any excess dye. Following that, the slides were washed with PBS three times. Hematoxylin solution was applied to stain the nuclei for 1 min, and the slides were fixed using 90 % glycerin.

*Determination of triglyceride level in the mouse liver*

The mouse livers from each group were weighed and placed into pre-cooled EP tubes containing 1 mL of PBS. The liver samples were homogenized for 15 sec, and the homogenate was transferred to a glass tube. To extract lipids, 4 mL of chloroform/methanol (2/1, v/v) was added to the tube. The mixture was then centrifuged at 300 × g and 4 °C for 30 min. The upper aqueous phase was carefully transferred to a new tube, and the above steps were repeated. The lower organic phase from both extractions was combined into another glass tube. The organic phase was dried under nitrogen, and 500 μL of a 3 % Triton X-100 (v/v) solution was added to dissolve the lipids. The levels of triglycerides (TG) in the liver tissues were determined following the instructions provided with the triglycerides kit (A110-1–1, Nanjing Jiancheng Bioengineering Institute, China). The TG values were normalized to the weight of the liver tissues.

*Determination of triglyceride level in the mouse serum*

Blood samples were collected from the mice after a 12-hour fasting period. The collected blood was then centrifuged at 1400 × g for 10 min at 4 °C. The resulting supernatant, which contained serum, was carefully collected for further analysis. The serum samples were used to measure the levels of serum triglycerides (TG) following the instructions provided with the triglycerides kit the same as 2.7.

*RNA isolation and real-time quantitative PCR*

Total RNA was extracted from liver samples or cells using TRIzol reagent according to the manufacturer's instructions. cDNA synthesis was performed using the All-In-One RT MasterMix (5 × ) kit. The mRNA expression levels were analyzed using SYBR Green quantitative PCR (qPCR) master mix. The primer sequences used in the RT-qPCR analysis can be found in Table 2.

*Protein isolation and Western blot*

Proteins from liver tissues and cells were isolated using radioimmunoprecipitation assay buffer (RIPA buffer), and the protein concentration was determined using the bicinchoninic acid (BCA) protein assay. The proteins were separated by 10 % SDS-PAGE and transferred to a nitrocellulose membrane. The membranes were incubated overnight at 4 °C with primary antibodies, including rabbit anti-COL1A1 (CST, #72026S, diluted at 1:1000), anti-α-SMA (CST, #19245, diluted at 1:2000), anti-COL1A2 (Immunoway, #YT6135, diluted at 1:1000), anti-BAX (CST, #2772, diluted at 1:1000), anti-BCL2 (CST, #3498, diluted at 1:1000), anti-CASP3 (Proteintech, #82202–1-RR, diluted at 1:1000), anti-FXR (Proteintech, #25055–1-AP, diluted at 1:1000), anti-CES1 (Proteintech, #16912–1-AP, diluted at 1:1000), and mouse anti-GAPDH (CST, #2118, diluted at 1:5000), anti-CASP8/p43/p18 (Proteintech, #13423–1-AP, diluted at 1:1000), anti-β-actin (Proteintech, #81115–1-RR, diluted at 5:1000). After primary antibody incubation, the membranes were incubated with horseradish peroxidase (HRP)-conjugated secondary antibodies for 1 h. Protein bands were visualized using an electrochemiluminescence system (BioRad, USA) and quantified using ImageJ software.

**Table 2**
Primer sequences used for q-PCR.

| Gene | | Sequence |
|---|---|---|
| *m-ACTA2* | Forward | CTACCACCATGTACCCAGGC |
| | Reverse | GAAGGTAGACAGCGAAGCCA |
| *m-COL1A1* | Forward | GCTCCTCTTAGGGGCCACT |
| | Reverse | CCACGTCTCACCATTGGG |
| *m-COL3A1* | Forward | CTGTAACATGGAAACTGGGGAAA |
| | Reverse | CCATAGCTGAACTGAAAACCACC |
| *m-TNFa* | Forward | AGCCAGGAGGGAGAACAGAAA |
| | Reverse | GCCACAAGCAGGAATGAGAAGA |
| *m-CCL2* | Forward | TTAAAAACCTGGATCGGAACCA |
| | Reverse | GCATTAGCTTCAGATTTACGGGT |
| *m-F4/80* | Forward | CCCCAGTGTCCTTACAGAGTG |
| | Reverse | GTGCCCAGAGTGGATGTCT |
| *h-FXR* | Forward | CCAGGGCTGCTTTTAACTC |
| | Reverse | GCTCCCCCCTGCAAATGA |
| *m-FXR* | Forward | TGGGCTCCGAATCCTCTTAGA |
| | Reverse | TGGTCCTCAAATAAGATCCTTGG |
| *m-GAPDH* | Forward | AAATGGTGAAGGTCGGTGT |
| | Reverse | AACTTGCCGTGGGTAGAGTC |
| *m-SHP* | Forward | CACCTGCATCTCACAGCCACT |
| | Reverse | GCCAACCCAAGCAGGAAGA |
| *m-ACC1* | Forward | CTTCCTGACAAACGAGTCTGG |
| | Reverse | CTGCCGAAACATCTCTGGGA |
| *m-FASN* | Forward | GGAGGTGGTGATAGCCGGTAT |
| | Reverse | TGGGTAATCCATAGAGCCCAG |
| *m-SREBP1c* | Forward | GATGCGAACTGGACACAG |
| | Reverse | CATAGGGGGCGTCAAACAG |

*Determination of hydroxyproline content in the mouse liver*

50 mg of mouse liver tissue was taken and placed in a 1.5 mL EP tube, 500 μL of 6 mol/L hydrochloric acid was added and digested at 100℃ for 4 h until no large tissue mass was visible. After cooling, 250 μL of 10 mol/L sodium hydroxide solution was added to adjust the pH to 6–8 and then filtered through a 70 μm membrane. The hydroxyproline (HYP) content was determined using the hydroxyproline kit (BC0250) from Beijing Solarbio (Beijing, China)

*Surface plasmon resonance assay*

The intermolecular interaction between HO and FXR proteins was analysed by surface plasmon resonance at 25 °C using the Biacore T200 system, a molecular interaction instrument. The purified FXR protein (Recombinant human Farnesoid X receptor (FXR) protein (17624-H07E): Beijing Yichiao Shenzhou Technology Co.) was dissolved in sodium acetate at pH 4.0 to 20 μg/mL, and then the purified FXR protein was attached to a CM5 dextran chip by amino coupling, resulting in 11,200 resonance units (RUs) of protein immobilised on a CM5 dextran chip. Concentration gradients of the HO drug solution were 200, 100, 50, 25, 12.5, 6.25, 3.125, 1.5625, 0 μmol/L. The flow rate was 30 μmol/L. Binding and dissociation were performed at a flow rate of 30 μL/min for 60 s each. Data were collated and analyzed using T200 version 3.1 evaluation software. The dissociation constants of HO and FXR were calculated by kinetic analysis and intermolecular interactions were assessed.

*Determination of HO concentrations in mouse plasma*

Oleanolic acid was used as an external standard, chromatographic grade ethyl acetate containing 100 ng/mL oleanolic acid

was prepared from which 1000 ng/mL HO solution was prepared. Gradient dilutions were performed to obtain 9 concentration gradients of 1000, 500, 250, 125, 62.5, 31.25, 15.625, 7.8 and 0 ng/mL HO ethyl acetate solution. Male C57BL/6J mice of the same background and body weight as those used in the animal study were used. After a single gavage administration of 100 mg/kg HO, 40–60 μL of blood was collected from the canthus at 0.5, 1, 2, 3, 4, 6, 8 and 24 h, and approximately 20 μL of plasma was centrifuged. Add 40 μL ethyl acetate containing the external standard to 20 μL plasma and mix thoroughly. 20 μL of blank plasma was taken from the standard and 40 μL of ethyl acetate solution containing different concentrations of HO was added. Centrifugation was performed at 13000 rpm for 10 min. 40 μL methanol was added to the supernatant and the supernatant was mixed thoroughly and centrifuged again at 10,000 rpm for 10 min. The supernatant was dried at 45 °C and then re-solubilised in methanol. The supernatant was dried at 45 °C, reconstituted in methanol and the drug concentration was determined by liquid chromatography-mass spectrometry (LC-MS/MS).

### *Statistical analysis*

Statistical analysis was conducted using Prism 8.0 software. The experimental data are presented as mean ± standard deviation (mean ± SD). The differences between the two groups were evaluated using a *t*-test, and differences among multiple groups were analyzed using one-way ANOVA. A p-value less than 0.05 was considered statistically significant.

## Results

### *HO inhibits hepatic lipid deposition and inflammation in the NASH mice induced by HFD + $CCl_4$*

Our previous study showed that HO was able to inhibit oleic acid-induced lipid deposition in hepatocytes[15]. In order to ascertain whether HO exerts an ameliorating effect on NASH, the highest gavage dose of 100 mg/kg/day was selected and *in vivo* pharmacokinetic assay was performed at first. The result is shown in Figure S1A, and the related parameters are presented in Figure S1B, which demonstrated that through gavage administration, HO could effectively absorb into the mouse bloodstream. Therefore, gavage administration was employed for the subsequent *in vivo* studies of HO.

To clarify the effect of HO on NASH, as illustrated in Fig. 1A, a NASH mouse model was constructed by HFD feeding in conjunction with intraperitoneal injection of $CCl_4$ for 8 weeks, with HO administered at high, medium, and low doses. The body weight, serum AST and ALT were increased after 8 weeks of HFD + $CCl_4$ treatment (Fig. 1B-D). HO treatment significantly inhibited HFD + $CCl_4$-induced increase of body weight, serum AST and ALT (Fig. 1B-D). Histologically, H&E and Oil Red O staining revealed fat vacuoles and droplets in hepatocytes of mice challenged with the HFD + $CCl_4$, and which were significantly reduced in the HO treatment group in a dose-dependent manner (Fig. 1E). The histological results were corroborated by the observation that HO treatment also significantly reduced triglyceride (TG) levels in mouse liver and serum (Fig. 1F). Furthermore, the qPCR results demonstrated that HO treatment down-regulated the mRNA expression of fatty acid synthesis-related genes (*SREBP1c* and *FASN*) and inflammation-related genes (*TNFα* and *CCL2*) as well as macrophage marker *F4/80* (Fig. 1G-H). The findings indicate that HO has the capacity to alleviate hepatic lipid deposition and inflammation in NASH mice.

### *HO inhibits liver fibrosis in the HFD + $CCl_4$-induced NASH mice*

Fibrosis represents a hallmark pathological feature of NASH disease progression. By staining liver tissue with Sirius Red, we found that HO was able to dose-dependently inhibit collagen deposition (Fig. 2A-B). Furthermore, in the model group, hydroxyproline, the main component of liver tissue collagen, was significantly elevated, and HO treatment significantly reduced this alteration (Fig. 2C). The qPCR analysis additionally demonstrated that HO was capable of inhibiting the mRNA expression levels of fibrosis-related genes (*ACTA2*, *COL1A1* and *COL3A1*) (Fig. 2D). Further examination of fibrosis-related proteins revealed that HO treatment significantly inhibited COL1A2 and α-SMA (Fig. 2E). These results reveal that HO has the potential to mitigate fibrosis in NASH.

### *HO inhibits liver fibrosis in the $CCl_4$-induced mice*

To further clarify the function of HO in the inhibition of liver fibrosis caused by hepatocyte injury and apoptosis, a fibrosis mouse model was constructed by IP injection of $CCl_4$ for 2 weeks, and 100 mg/kg/day of HO was administered (Fig. 3A). The results of serum transaminase analysis demonstrated that HO significantly reduced the plasma ALT and AST levels (Fig. 3B). The $CCl_4$-induced mice exhibited slight lipid deposition, and HO treatment was found to attenuate lipid deposition in the livers of mice, as indicated by H&E and Oil Red O staining (Fig. 3C). Consistently, HO also notably reduced serum and liver TG levels (Fig. 3D). Next, the qPCR assays revealed that HO treatment markedly decreased the hepatic mRNA levels of fatty acid synthesis-related genes (*SREBP1c* and *FASN*) and fibrosis-related genes (*ACTA2, COL1A1* and *COL3A1*) (Fig. 3E-F). Similarly, Western blot assay demonstrated that HO treatment effectively suppressed the upregulated protein expression levels of COL1A2 and α-SMA (Fig. 3G). This result was further confirmed by the results of Sirius red staining of the liver sections (Fig. 3C). The above results suggest that HO exerts an inhibitory effect on $CCl_4$-induced liver fibrosis.

### *HO attenuates hepatic stellate cell activation by inhibiting hepatocyte apoptosis*

In NASH, hepatocyte apoptosis is the initiator of fibrogenesis, which mainly includes endogenous apoptosis of hepatocytes induced by lipotoxicity and exogenous apoptosis induced by apoptotic signaling. In addition, the activated HSCs are the main effector cells for extracellular matrix production. To clarify the specific cells on which HO acts, we first explored the effect of HO on HSC activation in TGF-β-induced LX2 cells (Fig. 4A). The result of the Western blot assay demonstrated that the HO treatment did not inhibit the protein expression of COL1A1 in HSCs (Fig. 4B). Therefore, we proceeded to construct a hepatocyte apoptosis model utilizing PA, or TNF-α and Act D (Fig. 4C). In the PA-induced hepatocyte apoptosis model, HO was observed to significantly inhibit the protein level of c-CASP3 (Fig. 4D), and apoptotic cell staining by Annexin V-FITC/PI and sorting by flow cytometry also demonstrated that HO inhibited hepatocyte apoptosis (Fig. 4E). Furthermore, in the TNFα + Act-D-induced hepatocyte apoptosis model, HO significantly inhibited the protein level of c-CASP3 and c-CASP8 (Fig. 4F). To further elucidate the potential inhibitory effect of HO on HSC activation, we constructed a hepatocyte-HSC interaction model and investigated the impact of HO on this process (Fig. 4G). Our findings demonstrated that the protein expression of COL1A1 in LX2 cells was significantly reduced in the HO-treated group (Fig. 4H). In order to further elucidate the inhibitory effect of HO on hepatocyte apoptosis *in vivo*, we examined the expression of apoptosis-related proteins in the liver tissues from the $CCl_4$-induced mice as well as the HFD + $CCl_4$-induced model. The results demonstrated that HO

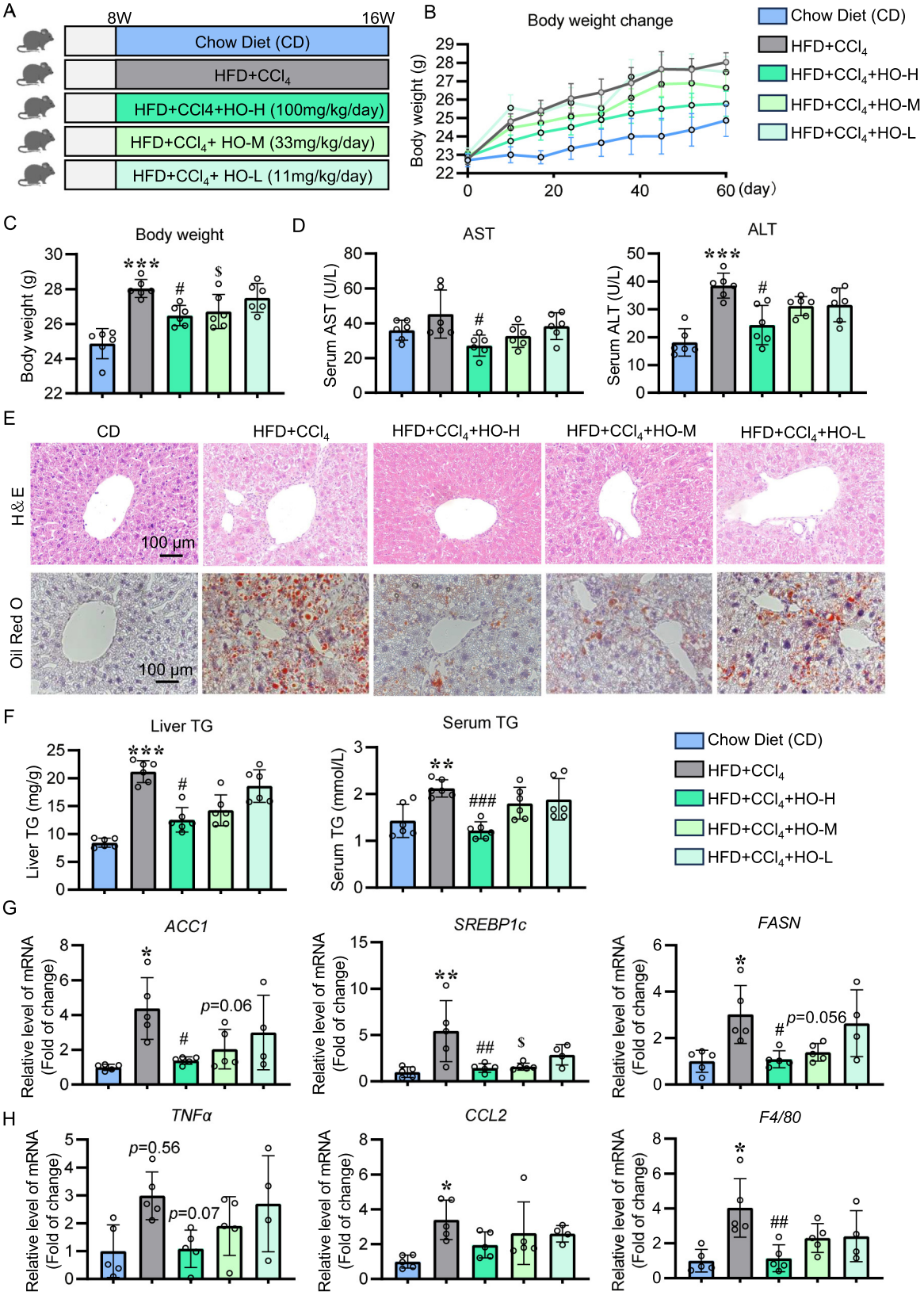


**Fig. 1. HO inhibits hepatic lipid deposition and inflammation in the NASH mice induced by HFD + $CCl_4$.** (A) The flow chart for the effects of HO on HFD + $CCl_4$-induced NASH fibrosis in WT mice. (B) Body weight change during the modeling. (C) Body weight of mice. (D) ALT and AST levels in serum. (E) Representative histological images of H&E, Oil Red O and Sirus Red staining of mouse liver sections from the indicated groups. Scale bar = 100 μm. (F) TG contents in the mouse livers and serums. (G) Hepatic mRNA expression levels of the genes related to lipid metabolism. (H) Hepatic mRNA expression levels of the genes related to inflammation. N = 5 ~ 6. */#/$/&$P < 0.05$, **/##/$/&&$P < 0.01$, ***/###/$$$/&&&$P < 0.001$.* HFD + $CCl_4$ *vs* CD; # HFD + $CCl_4$ *vs* HFD + $CCl_4$ + HO-H; $ HFD + $CCl_4$ *vs* HFD + $CCl_4$ + HO-M; & HFD + $CCl_4$ *vs* HFD + $CCl_4$ + HO-L. (For interpretation of the references to colour in this figure legend, the reader is referred to the web version of this article.)

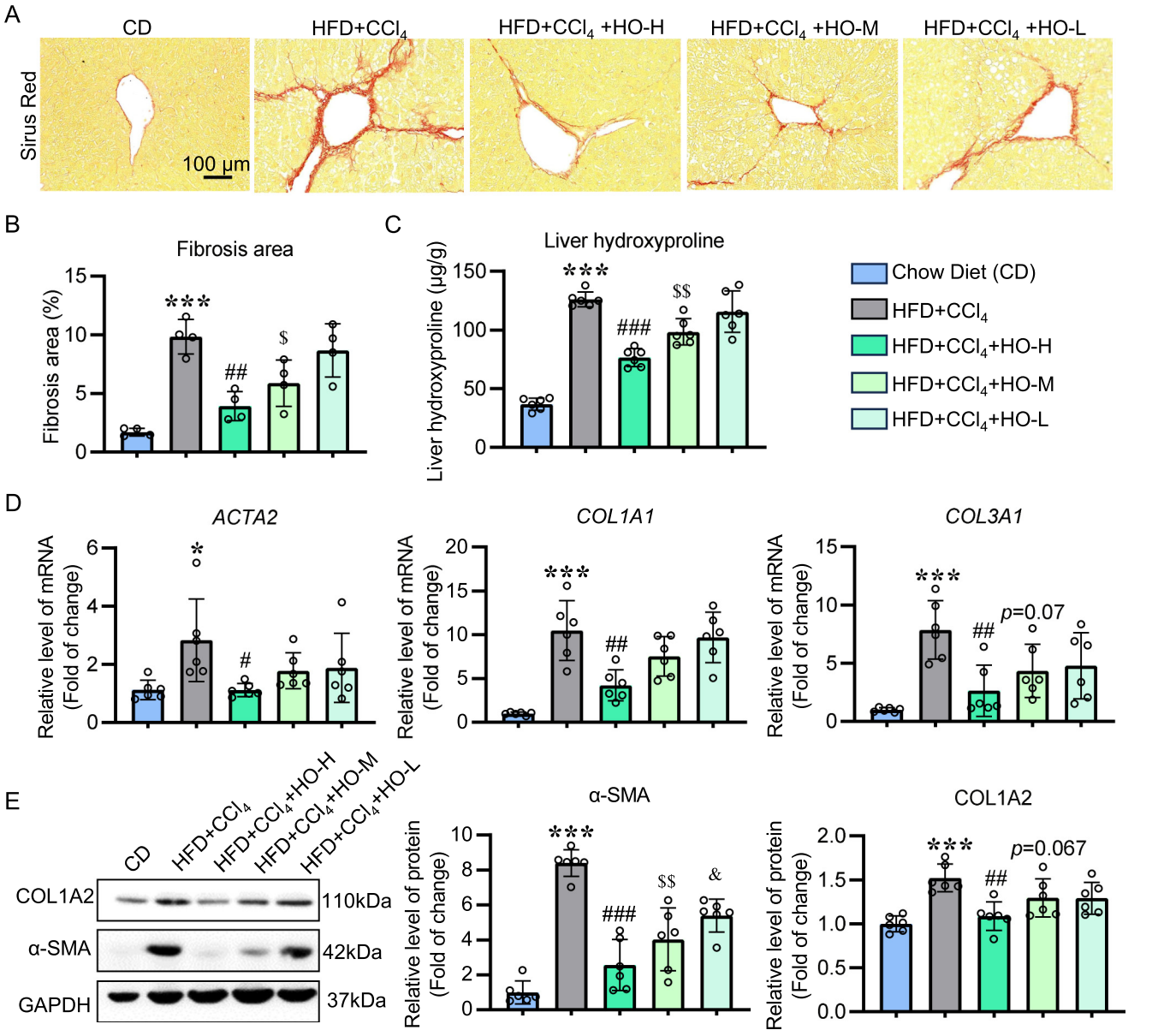


**Fig. 2. HO inhibits liver fibrosis in the HFD + $CCl_4$-induced NASH mice.** (A) Representative histological images of Sirius Red staining of mouse liver sections from the indicated groups, Scale bar = 100 μm.(B) The percent (%) positive PSR area measured on Image J. Scale, N = 4. (C) Hydroxyproline contents in the mouse livers. (D) Hepatic mRNA levels of the genes related to fibrosis. (E) Western blot and quantification of proteins related to fibrosis in mouse livers from the indicated groups. N = 5 ~ 6. */#/$/&$P$ < 0.05, **/##/&&$P$ < 0.01, ***/###/$$$/&&&$P$ < 0.001.* HFD + $CCl_4$ *vs* CD; # HFD + $CCl_4$ *vs* HFD + $CCl_4$ + HO-H; $ HFD + $CCl_4$ *vs* HFD + $CCl_4$ + HO-M; & HFD + $CCl_4$ *vs* HFD + $CCl_4$ + HO-L. (For interpretation of the references to colour in this figure legend, the reader is referred to the web version of this article.)

significantly upregulated the expression of the pro-apoptotic protein BAX and significantly inhibited the expression of the anti-apoptosis-related protein BCL2 (Fig. 5A-B). Furthermore, HO significantly inhibited the elevation of c-CASP 8 protein levels (Fig. 5A-B). The aforementioned results indicate that HO might play a role in the alleviation of NASH fibrosis by inhibiting hepatocyte apoptosis and thus suppressing HSC activation.

*HO targets and upregulates protein level of FXR*

In order to further explore the potential target of HO, we predicted the possible target set of HO based on its chemical structure through the Swiss Target Prediction website (https://swisstargetprediction.ch/). The results indicated that it was mainly enriched in nuclear receptors (Figure S2A). Next, the target proteins predicted by Swiss Target Prediction and SEA Search Server website (https://sea.bkslab.org/) were intersected with the targets of NASH and liver fibrosis in Gene Cards (https://www.genecards.org/), the result suggested that the nuclear receptors LXR and FXR may mediate the anti-NASH fibrotic effects of HO (Figure S2B). A comparison of the relevance scores for LXR and FXR in the context of NASH and liver fibrosis indicated that FXR plays a more significant role in the NASH fibrosis (Figure S2C). Furthermore, the binding relationship between HO and the two proteins was simulated using the molecular docking technique. The results demonstrated that the binding energy of HO to FXR was −9.3 kJ/mol (Fig. 6A), whereas that of LXR was −5.4 kJ/mol (Figure S2D), indicating that the binding ability of HO to FXR is stronger than to LXR. The direct binding of HO to the FXR protein was further proved by surface plasmon resonance assay, which yielded a $K_D$ value of 11 μmol/L (Fig. 6B).

Subsequently, we examined the mRNA expression levels of FXR and its target gene *SHP* in both the $CCl_4$ and HFD + $CCl_4$ mouse

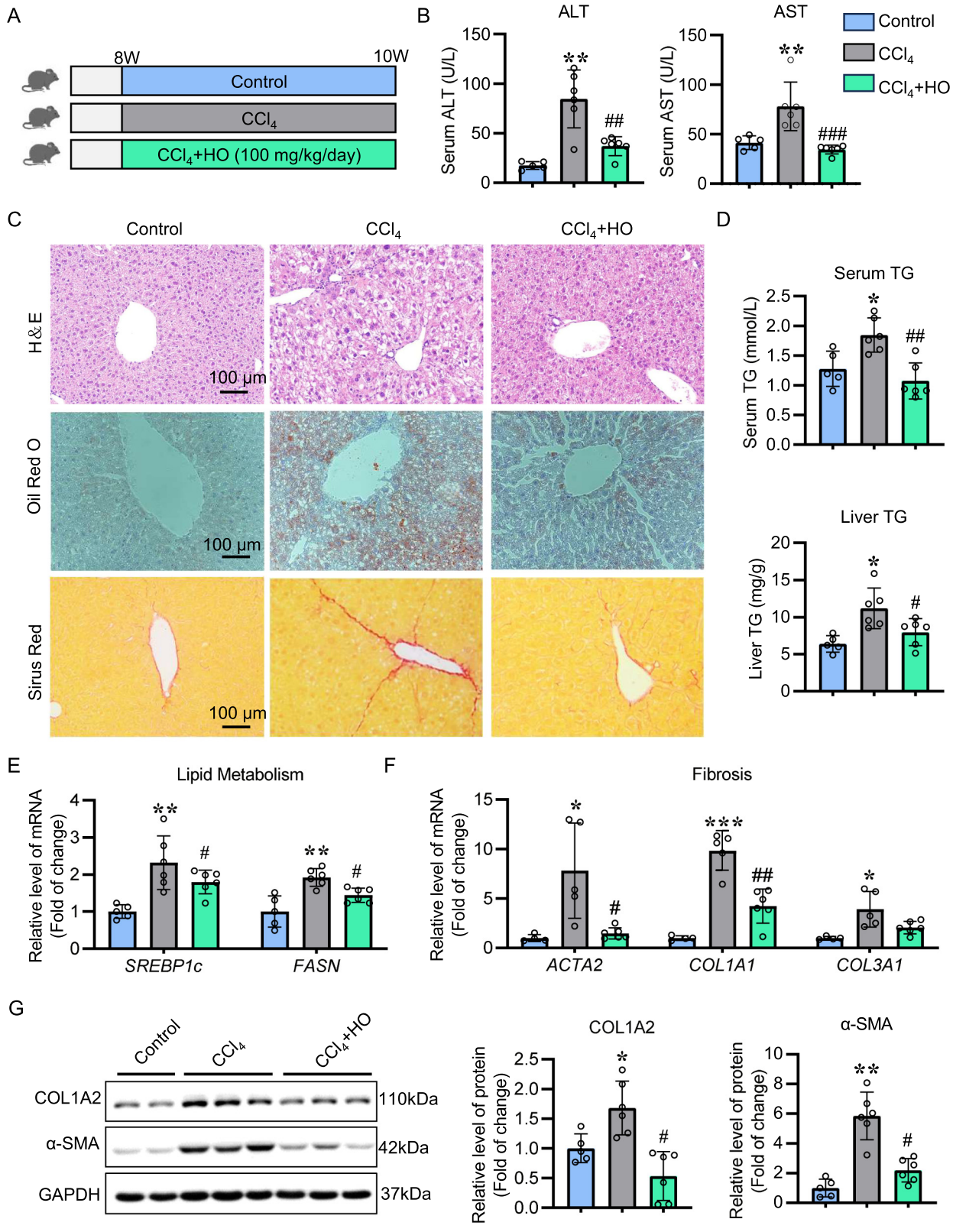


**Fig. 3. HO inhibits mouse liver fibrosis induced by $CCl_4$.** (A) The flow chart for the effects of HO on $CCl_4$-induced liver fibrosis in WT mice. (B) ALT and AST levels in mouse serums. (C) Representative histological images of H&E, Oil Red O and Sirus Red staining of mouse liver sections from the indicated groups. Scale bar = 100 μm. (D) TG contents in the mouse livers and serums. (E) Hepatic mRNA expression levels of the genes related to lipid metabolism. (F) Hepatic mRNA expression levels of the genes related to fibrosis. (G) Western blots and quantification of proteins related to fibrosis in mouse livers from the indicated groups. N = 5 ~ 6. */#$P < 0.05$, **/##$P < 0.01$, ***/###$P < 0.001$.* $CCl_4$ *vs* Control; # $CCl_4$ *vs* $CCl_4$ + HO. (For interpretation of the references to colour in this figure legend, the reader is referred to the web version of this article.)

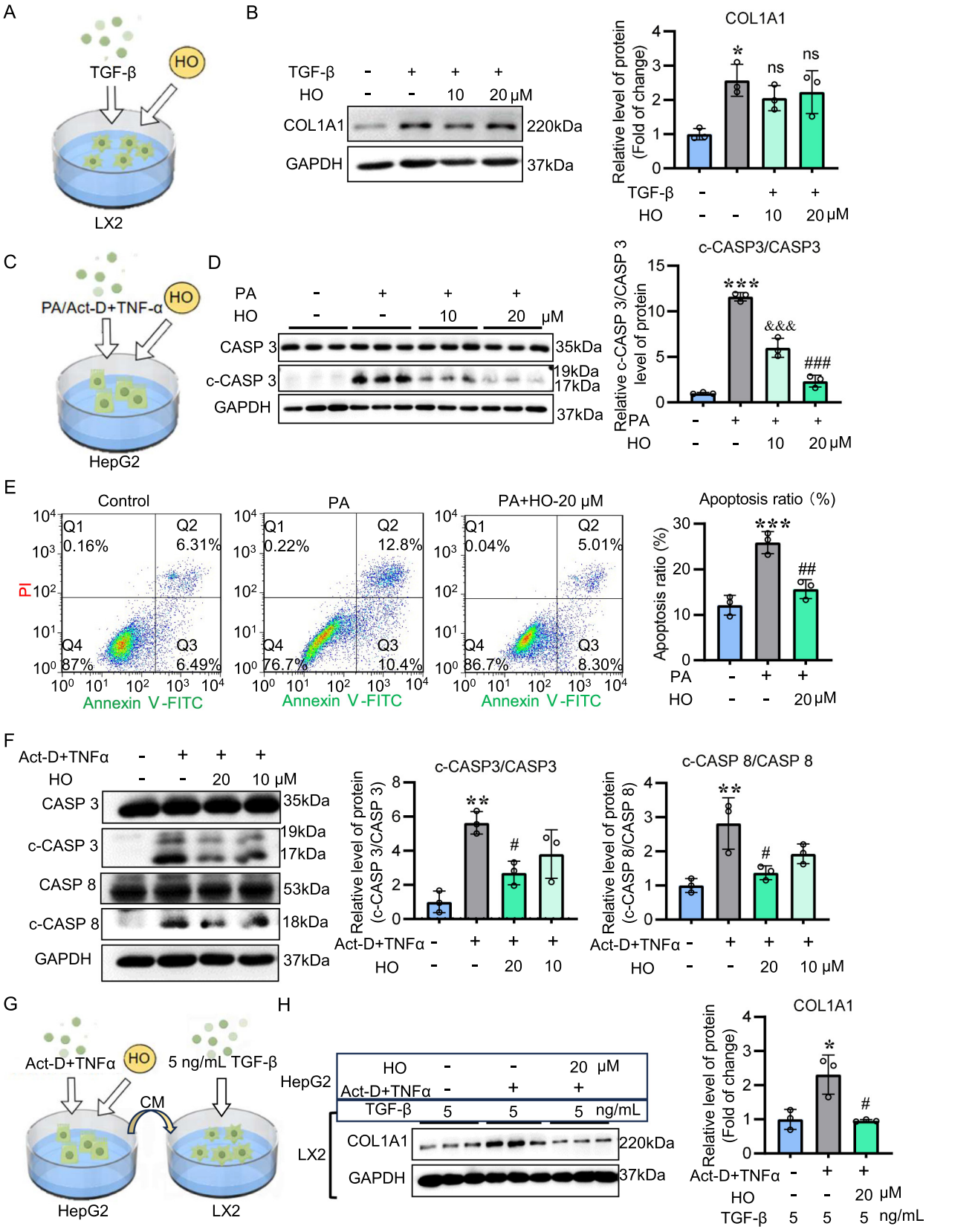


**Fig. 4. HO attenuates hepatic stellate cell activation by inhibiting hepatocyte apoptosis.** (A) The flow chart for the effects of HO on TGF-β-induced HSCs activation in LX2 cells. (B) Western blot and quantification of COL1A1 protein in LX2 cells. (C) The flow chart for the effects of HO on PA/TNFα + Act-D-induced hepatocyte apoptosis in HepG2 cells. (D) Western blot and quantification of c-CASP3 protein in HepG2 cells. (E) Apoptosis proportions of HepG2 cells analyzed by flow cytometry. (F) Western blot and quantification of the proteins of c-CASP3 and c-CASP8 in HepG2 cells. (G) The flow chart for the effects of HO on hepatocyte apoptosis-HSC activation interaction. (H) Western blot and quantification of COL1A1 protein in LX2 cells. N = 3. */#/&$P$ < 0.05, **/##/&&$P$ < 0.01, ***/###/&&&$P$ < 0.001.* Model *vs* Control; # Model *vs* Model + HO-20; Model *vs* Model + HO-10.

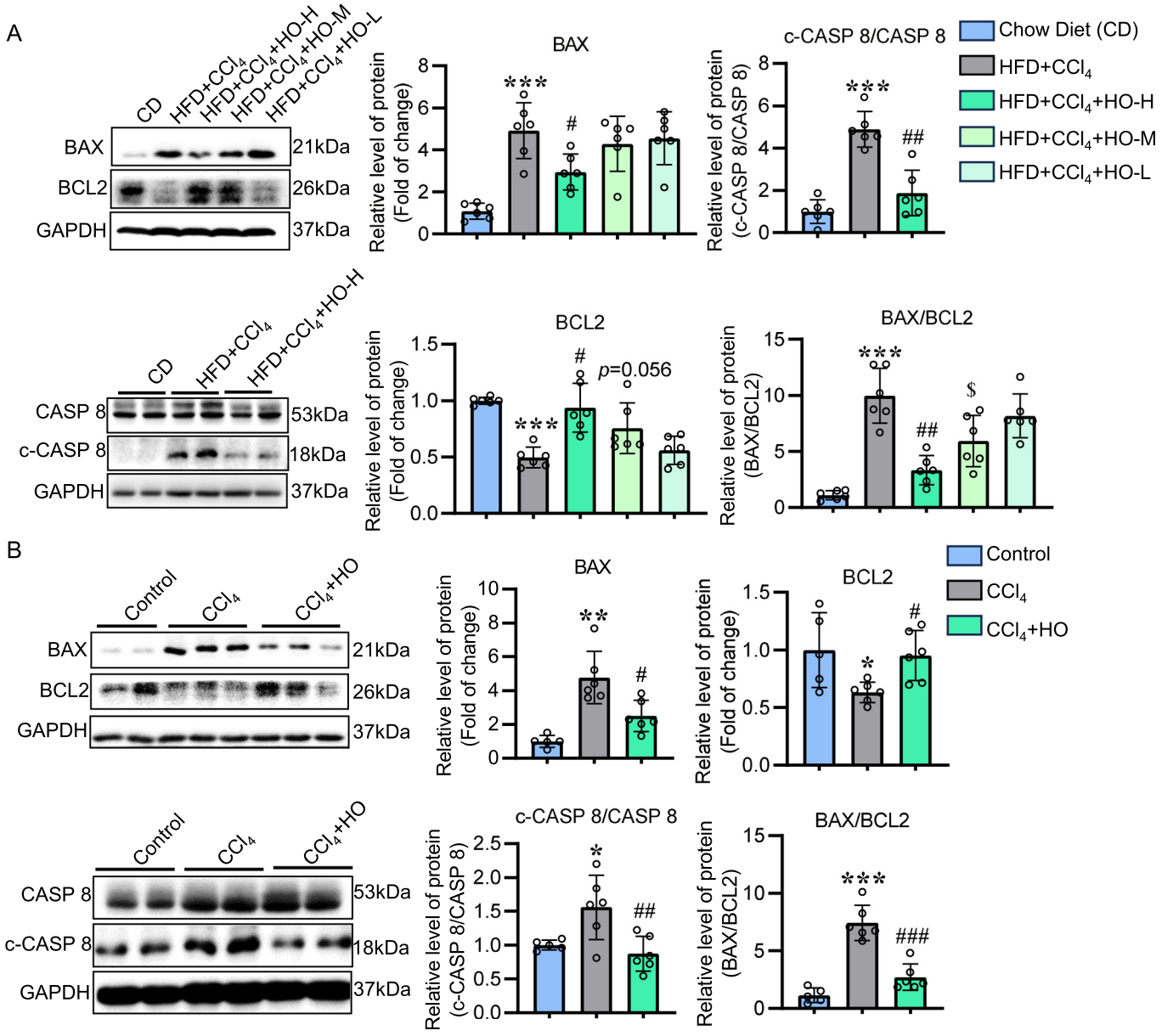


**Fig. 5. HO inhibits apoptosis level in the mouse livers.** (A) Western blot and quantification of the proteins of BAX, BCL2 and c-CASP8 in the livers of HFD + $CCl_4$-induced NASH fibrosis in mice. (B) Western blot and quantification of the proteins of BAX, BCL2 and c-CASP8 in the livers of $CCl_4$-induced liver fibrosis in mice. N = 5 ~ 6. */#/&$P$ < 0.05, **/##/&&$P$ < 0.01, ***/###/&&&$P$ < 0.001. * HFD + $CCl_4$ *vs* CD or $CCl_4$ *vs* Control; # HFD + $CCl_4$ *vs* HFD + $CCl_4$ + HO-H or $CCl_4$ *vs* $CCl_4$ + HO; $ HFD + $CCl_4$ *vs* HFD + $CCl_4$ + HO-M; & HFD + $CCl_4$ *vs* HFD + $CCl_4$ + HO-L.

models. Our findings demonstrated that HO treatment had no effect on the mRNA level of *FXR* in the mouse livers, but significantly upregulated the mRNA expression level of *SHP* (Fig. 6C and E). Furthermore, the results of the Western blot demonstrated that treatment with HO significantly upregulated FXR protein levels in both mouse models, and the upregulation of the FXR protein levels by HO was also confirmed *in vitro* on PA and TNFα + Act-D-induced hepatocyte apoptosis models (Fig. 6D and F-H). Furthermore, how HO impacts the FXR protein level was investigated by inhibiting protein synthesis, and the results demonstrated that HO upregulated the protein level of FXR at the basal level and significantly prolonged the half-life of FXR protein (Fig. 6I).

FXR has been reported to protect hepatocytes by inhibiting lipid deposition, which is partly dependent on its downstream gene CES1[11]. Our results demonstrated that CES1 protein levels were significantly reduced in the model group, and HO treatment was able to reverse the alteration (Fig. 6J-K).

The above results suggest that HO exerts an inhibitory effect on hepatocyte apoptosis and NASH fibrosis by binding to and upregulating the protein level of FXR in hepatocytes. This effect is partially dependent on FXR's downstream genes of *SHP* and *CES1*.

### *The inhibition of hepatocyte apoptosis by HO is dependent on FXR*

To ascertain whether hepatocyte FXR is involved in the pharmacological effects of HO, we employed the Cre-loxP recombinase system to specifically knockout of FXR in mouse hepatocytes, thereby obtaining hepatocyte FXR-specific knockout mice ($FXR^{KO}$) and their littermate control mice ($FXR^{WT}$) (Figure S3A). The mouse genotypes were confirmed by collecting mouse tail samples at three weeks of age for genotyping (Figure S3B). The protein expression levels of FXR and the mRNA expression levels of its target gene *SHP* were further examined to ensure that FXR was successfully knocked out in the mouse livers. The results demonstrated that

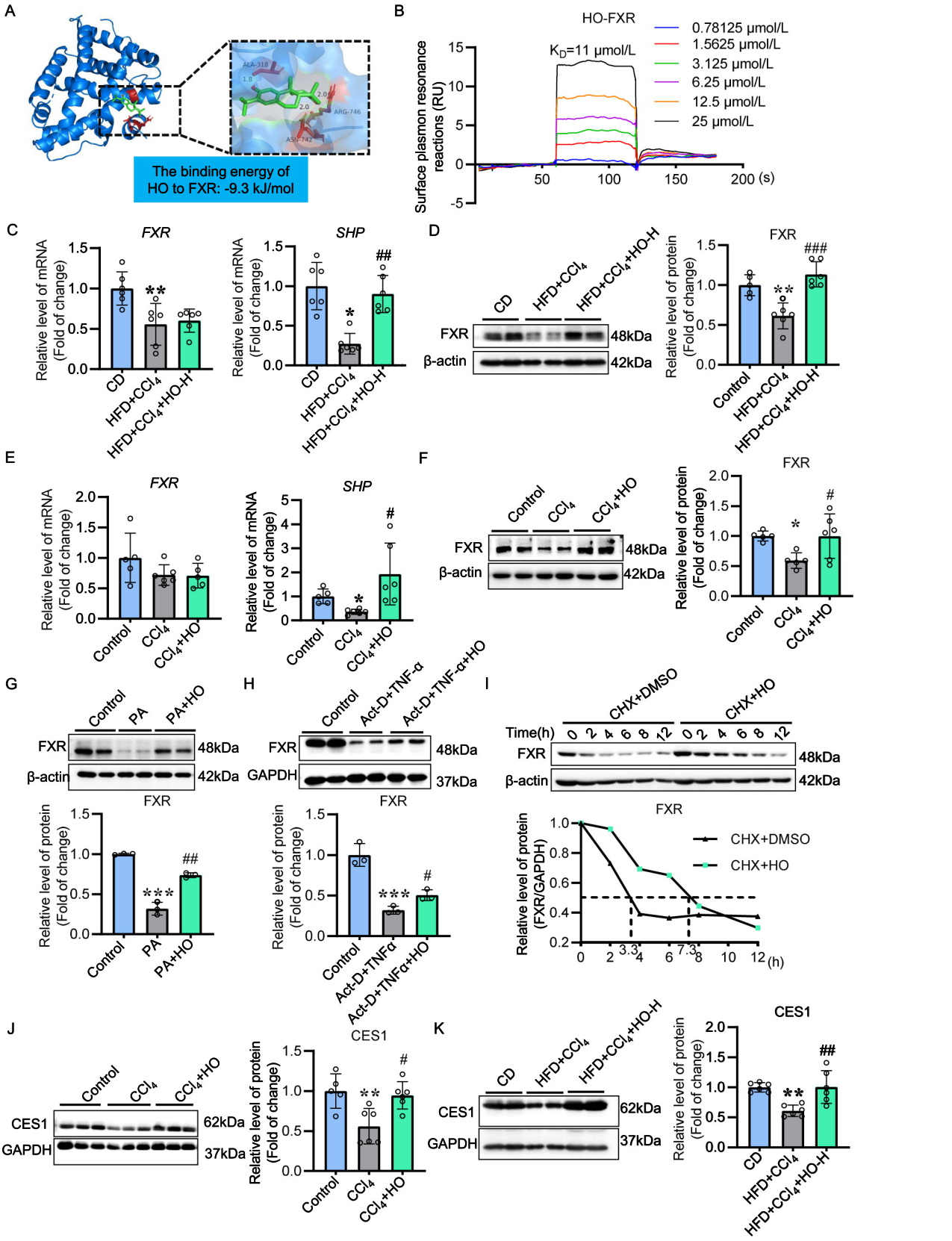


**Fig. 6. HO targets to and upregulates protein level of FXR.** (A) HO-FXR molecular docking by Auto Dock. (B) Surface plasmon resonance results for HO and FXR. (C) Hepatic mRNA levels of the genes of FXR and SHP in HFD + $CCl_4$-induced NASH fibrosis in mice. (D)Western blot and quantification of the hepatic FXR protein in HFD + $CCl_4$-induced NASH fibrosis in mice. (E) Hepatic mRNA levels of the genes of FXR and SHP in $CCl_4$-induced liver fibrosis in mice. (F)Western blot and quantification of the hepatic FXR protein in $CCl_4$-induced liver fibrosis mice. (G) Western blot and quantification of FXR protein in PA-induced hepatocyte apoptosis. (H) Western blot and quantification of FXR proteinin TNFα + Act-D-induced hepatocyte apoptosis. (I) Western blot and quantification of FXR protein in protein degradation experiment. (J) Western blot and quantification of the hepatic CES1 protein in HFD + $CCl_4$-induced NASH fibrosis in mice. (K) Western blot and quantification of the hepatic CES1 protein in $CCl_4$-induced liver fibrosis in mice. N = 3 in *in vitro* studies; N = 5 ~ 6 in *in vivo* studies. */#$P$ < 0.05, **/##$P$ < 0.01, ***/###$P$ < 0.001.* Model *vs* Control; # Model *vs* Model + HO/HO-H.

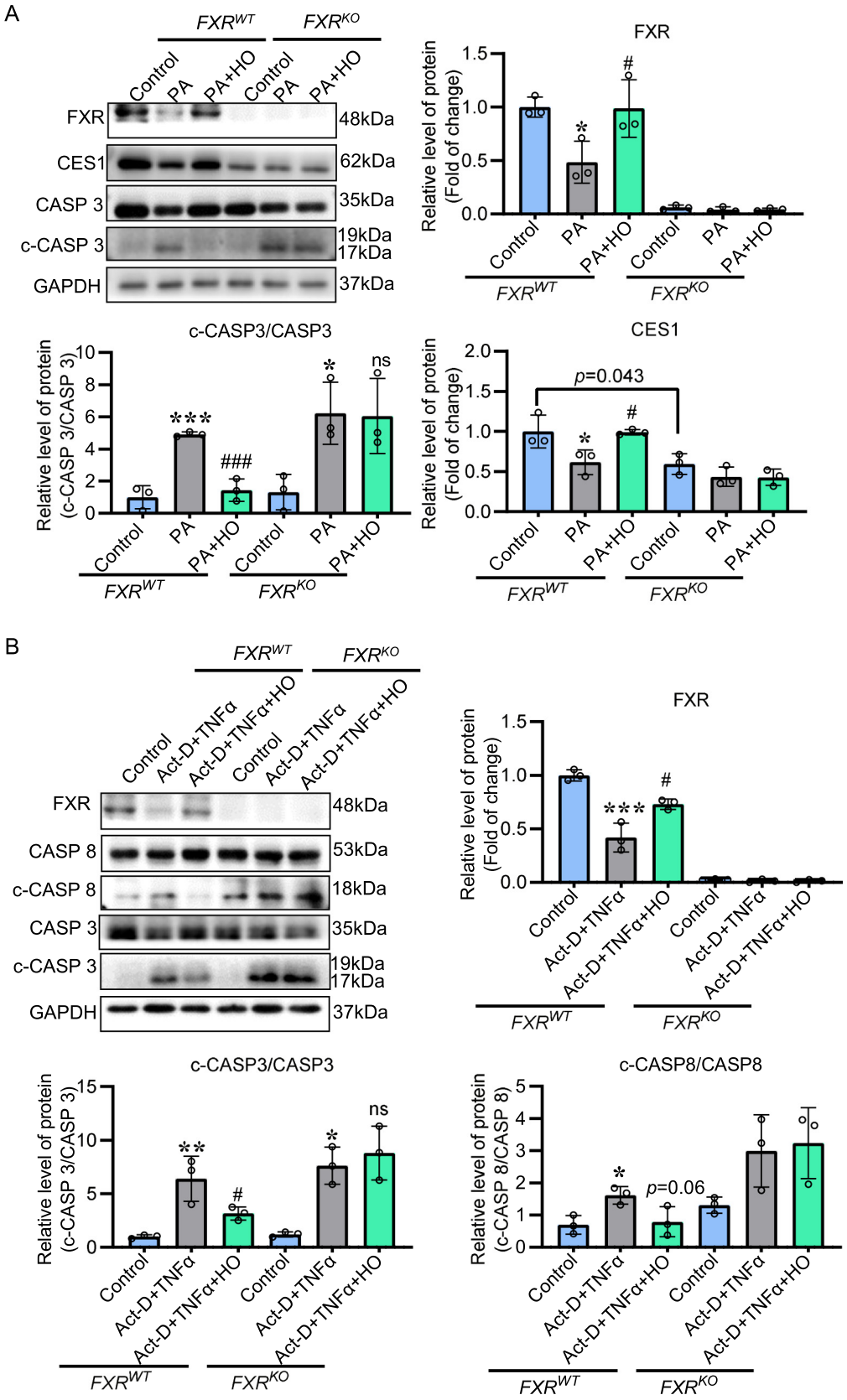


**Fig. 7. The inhibition of hepatocyte apoptosis by HO is dependent on FXR.** (A) Western blot and quantification of FXR, CES1 and c-CASP3 proteins in PA-induced apoptosis in primary hepatocytes extracted from the $FXR^{WT}$ or $FXR^{KO}$ mice. (B) Western blot and quantification of FXR, c-CASP8 and c-CASP3 proteins in Act-D + TNFα-induced apoptosis in primary hepatocytes extracted from the $FXR^{WT}$ or $FXR^{KO}$ mice. N = 3. */#$P < 0.05$, **/##$P < 0.01$, ***/###$P < 0.001$.* Model *vs* Control; # Model *vs* Model + HO.

Fig.8

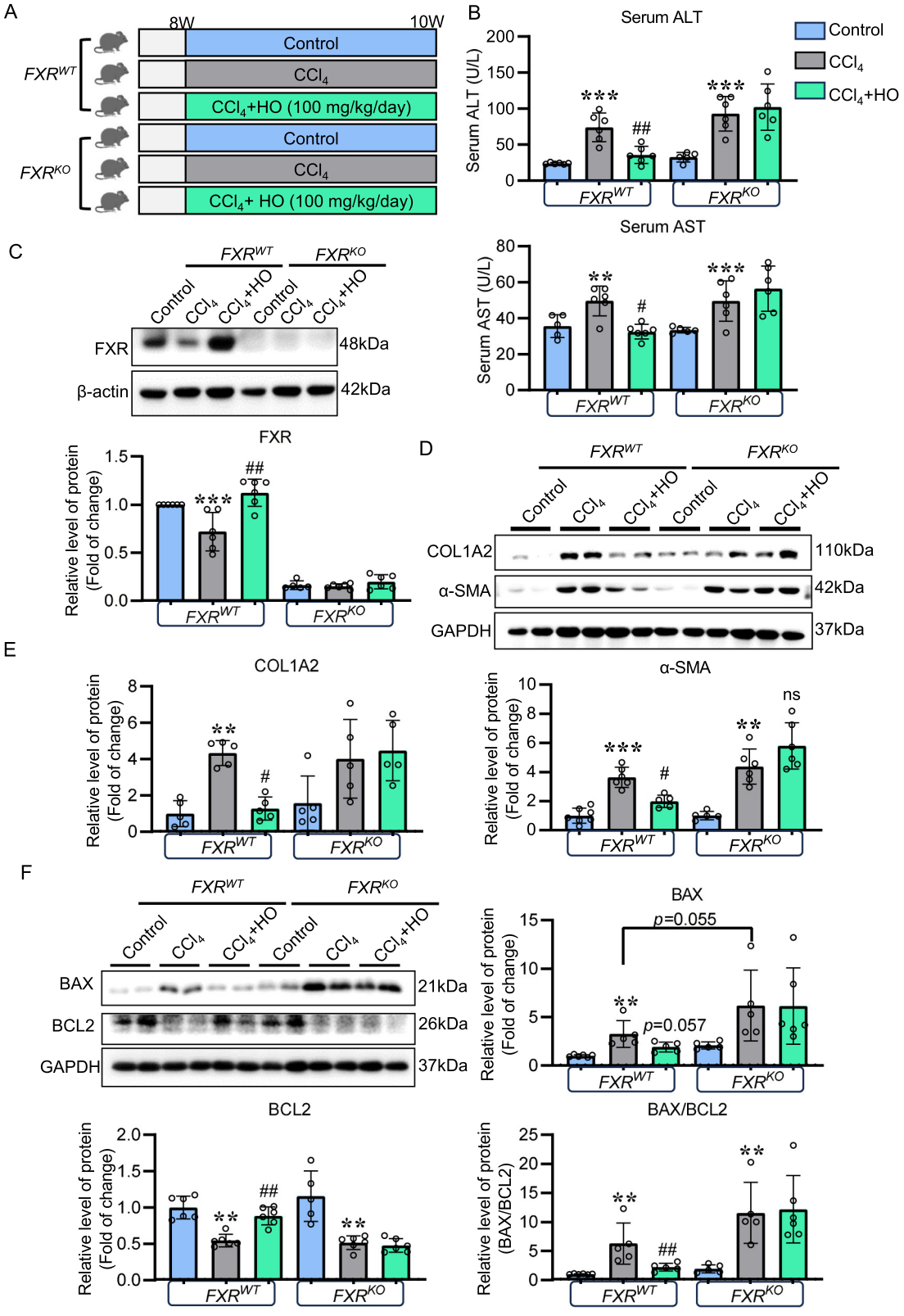


**Fig. 8. HO's inhibition effect of liver fibrosis is mediated by the hepatocyte FXR.** (A) The flow chart for the effects of HO on $CCl_4$-induced liver fibrosis in the $FXR^{WT}$ and $FXR^{KO}$ mice. (B) ALT and AST levels in the mouse serums. (C)Western blot and quantification of FXR protein in the livers of $FXR^{WT}$ and $FXR^{KO}$ mice. (D)Western blot of COL1A2 and α-SMA in the livers of $FXR^{WT}$ and $FXR^{KO}$ mice. (E) The quantification of COL1A2 and α-SMA. (F) Western blot and quantification of BAX and BCL2 in the livers of $FXR^{WT}$ and $FXR^{KO}$ mice. N = 5 ~ 6. */#$P$ < 0.05, **/##$P$ < 0.01, ***/###$P$ < 0.001.* $CCl_4$ *vs* Control; # $CCl_4$ *vs* $CCl_4$ + HO.

the protein level of FXR and its target gene *SHP* were reduced in the liver tissues of $FXR^{KO}$ mice compared with those of $FXR^{WT}$ mice (Fig. S3C-D).

To clarify whether FXR mediates the inhibitory effect of HO on hepatocyte apoptosis, primary hepatocytes were extracted from both $FXR^{WT}$ and $FXR^{KO}$ mice and hepatocyte apoptosis models were established by either PA or Act-D + TNFα induction. The results of Western blot demonstrated that in the $FXR^{WT}$ hepatocytes, HO significantly upregulated the protein level of FXR and significantly suppressed the protein level of c-CASP 3, whereas this effect of HO was lost in $FXR^{KO}$ hepatocytes (Fig. 7A-B). Furthermore, HO treatment led to a notable elevation in the protein level of CES1 in the PA-induced hepatocyte apoptosis model (Fig. 7A). In the Act-D + TNFα-induced hepatocyte apoptosis model, HO treatment resulted in a significant inhibition of the upregulation of c-CASP 8 (Fig. 7B). The aforementioned effects were found to be absent following the knockout of FXR in hepatocytes (Fig. 7A-B), which indicates that the inhibition of hepatocyte apoptosis by HO is contingent upon FXR.

### *HO's inhibition effect of liver fibrosis is mediated by the hepatocyte FXR*

To further validate the mediating relationship of hepatocyte FXR with the inhibitory effect of HO on liver fibrosis *in vivo*, we established $CCl_4$-induced liver fibrosis in both $FXR^{WT}$ and $FXR^{KO}$ mice, and meanwhile treated the mice with HO (Fig. 8A). The results of the serum aminotransferase assays demonstrated that HO treatment significantly reduced the serum ALT and AST levels in the $FXR^{WT}$ mice, whereas it had no inhibitory effects on the elevated ALT and AST levels in the $FXR^{KO}$ mice (Fig. 8B). The results of Western blot demonstrated that in $FXR^{WT}$ mice, HO treatment significantly upregulated the protein levels of FXR as well as the anti-apoptosis-related protein BCL2, and significantly inhibited the levels of fibrosis-related proteins (α-SMA and COL1A2) and apoptosis-related protein (BAX). However, these effects were abolished in the $FXR^{KO}$ mice (Fig. 8C-F). The above results indicate that the protective effects of HO on the inhibition of hepatocyte apoptosis and thus suppression of liver fibrosis are dependent on the FXR in hepatocytes.

## Discussion

Early intervention in NASH fibrosis disease has a significant impact on improving the long-term prognostic outcome of patients. However, the treatment of NASH fibrosis remains challenging in clinical care. The pathogenesis of which involves hepatocyte injury and apoptosis caused by intracellular lipid overload, which initiates the development of fibrosis[18]. In addition to the direct activation of HSCs through apoptotic bodies and damage-associated molecular patterns, apoptosis of hepatocytes also triggers inflammatory responses, which exacerbate the activation of HSCs[19–21]. To emulate the disease process, we fed the mice with HFD to induce hepatic lipid deposition and concurrently IP injection of $CCl_4$ to accelerate hepatocyte injury and apoptosis, thereby exacerbating the fibrosis process. This mouse model was able to more accurately reflect the pathological features of human NASH and demonstrated fibrotic lesions within a relatively short period of time[22–24]. In this mouse model, we observed that HO dose-dependently inhibited hepatic lipid deposition, inflammation, and fibrosis. In addition, HO also exhibited inhibition of mouse liver fibrosis induced by $CCl_4$, which further suggests that HO ameliorates liver fibrosis by inhibiting hepatocytes injury and apoptosis and also indicates that HO may have a broad inhibitory effect on the liver fibrosis caused by multiple factors-induced injury and apoptosis in hepatocytes.

Hepatocyte apoptosis and HSC activation represent key pathological processes in the development of non-alcoholic steatohepatitis (NASH) fibrosis[25]. Studies have demonstrated that the hepatocyte injury and apoptosis resulting from lipid overload are pivotal factors in promoting NASH fibrosis[7]. Consequently, improving lipid deposition can inhibit hepatocyte apoptosis, which in turn retard the development of NASH fibrosis in mice[24]. Furthermore, the direct inhibition of HSC activation has been proposed as a potential therapeutic approach for the treatment of NASH fibrosis[26]. The results of our study indicated that HO does not exert a direct inhibitory effect on TGF-β-induced HSC activation. Consequently, we proceeded to construct a model of lipotoxic apoptosis and receptor-signaling apoptosis induced by PA and Act-D + TNFα, respectively. Our findings demonstrated that HO significantly inhibits hepatocyte apoptosis and consequently indirectly inhibits HSC activation by inhibiting hepatocyte apoptosis.

Mechanically, the results of molecular docking and SPR assay indicated the existence of direct binding of HO to FXR, suggesting that HO acts by targeting FXR. FXR represents a reliable target for disease intervention in NASH[27]. In the liver, FXR is mainly expressed in biliary epithelial cells and hepatocytes, with lower expression in HSCs and other cells[28]. Although some studies have demonstrated that FXR activation in HSCs can directly inhibit HSC activation by modulating lipid droplets in HSCs or interfering with the TGF-β signaling pathway, the experimental design of these studies did not exclude the potential role of FXR in hepatocytes[29,30]. In the liver, the number of hepatocytes and the expression of FXR are considerably higher than in HSCs. This may explain why no direct inhibition of HSC activation by HO treatment was observed in our study. To clarify whether FXR mediates the pharmacological effects of HO, we established apoptosis models on the primary hepatocytes isolated from the $FXR^{KO}$ mice, the results showed that the inhibitory effect of HO on hepatocyte apoptosis was absent. Furthermore, in the liver fibrosis model induced by $CCl_4$, we found that the absence of FXR in hepatocytes resulted in the loss of HO's function in inhibiting liver fibrosis and apoptosis on these mice. These findings suggest that hepatocyte FXR mediates the pharmacological efficacy of HO in inhibiting hepatocyte apoptosis and liver fibrosis, and that FXR is a pharmacological target of HO.

Our study revealed that HO did not regulate the mRNA levels of FXR, but significantly upregulated the FXR protein levels in hepatocytes. In order to ascertain the mechanism of this results, we used CHX to inhibit hepatocyte protein synthesis. And our findings demonstrated that HO treatment resulted in a significant prolongation of the half-life of FXR protein. This suggests that HO may upregulate FXR protein level by inhibiting FXR protein degradation. Furthermore, it has been demonstrated that silencing message regulators regulate the ubiquitination and degradation of FXR protein by controlling the nucleo-plasmic shuttling of FXR through the modulation of acetylation at the K217 site and phosphorylation at the T442 site of FXR[31,32]. It is proposed that HO binding to FXR may occupy some of the modification sites of FXR, thus affecting the degradation of FXR. The precise molecular mechanism by which HO upregulates the protein level of FXR will be elucidated in our follow-up study.

As a nuclear receptor, FXR regulates metabolic processes such as lipid synthesis and catabolism through transcriptional regulatory functions in hepatocytes. In the present study, we found that HO treatment enhances the regulation of FXR on its downstream target genes, *SHP* and *SREBP1c*, which has a beneficial effect on ameliorating hepatic lipid deposition. Besides, CES1 is highly expressed in hepatocytes, and upregulation of CES1 can increase the hydrolysis of triglyceride in hepatocytes, which alleviates the lipotoxic injury of hepatocytes[33–35]. It is reported that the promoter region of CES1 contains an FXR-binding element, and CES1

partially mediates the function of FXR to inhibit lipid deposition and protect hepatocytes[11]. In the present study, we observed that HO upregulated the protein expression levels of CES1, which may be part of the mechanism by which FXR inhibits hepatic lipid deposition and hepatocyte lipotoxic apoptosis.

Furthermore, existing studies have demonstrated that FXR can interact with CASP8 in the cytoplasm through a non-classical function, preventing assembly of the death receptor complex and inhibiting the cleavage of CASP 8 into the active c-CASP 8, thereby inhibiting the activation of downstream CASP 3 and CASP 7, interfering with apoptosis in the receptor pathway induced by apoptotic signals, and inhibiting the development of liver fibrosis[12]. The present study also demonstrated that HO was able to inhibit the protein level of c-CASP 8, the active form of the apoptotic molecular switch CASP 8, suggesting that HO may influence the binding of FXR to CASP8.

Based on the pivotal role of hepatocyte apoptosis in the progression of NASH fibrosis, a pan-CASP inhibitors was developed for the treatment of NASH fibrosis. However, clinical endpoints were not met, suggesting that direct inhibition of the apoptotic process in hepatocytes without exposure to the primary causative factors is not an effective means of ameliorating the pathological process[36,37]. The present study demonstrated that HO ameliorates hepatocyte lipid deposition by targeting FXR, which attenuates hepatocyte lipotoxic injury at the source, and consequently prevents hepatocyte apoptosis. As a result, mitigating NASH fibrosis by intervening in multiple pathological processes, which suggests a better therapeutic potential and clinical translational value of HO.

In addition, FXR agonists have been proven to improve NASH fibrosis by protecting hepatocytes in preclinical trials[10]. The bile acid analogue-obeticholic acid, a potent agonist of the FXR, exerts its effects by ligand-receptor binding, thereby promoting the transcriptional regulatory function of the FXR[38]. However, obeticholic acid did not meet the primary endpoint of regression of NASH fibrosis in its phase III clinical trial, which was associated with significantly lower hepatic FXR expression in the NASH patients than in healthy people[12,31]. Available studies have demonstrated that the inhibitory effect of FXR agonists on fibrosis can be significantly enhanced by overexpression or upregulation of FXR in hepatocytes, or by the concomitant use of FXR agonists [12,31,39]. The up-regulation of FXR protein level by HO in this study indicates that the combination of HO with FXR agonists may have the potential to enhance the anti-NASH fibrosis effect of the FXR agonists, thus achieving a more efficient therapeutic effect on NASH fibrosis than using FXR agonists alone. This may represent a potential strategy for addressing the practical challenges associated with FXR as a target for drug development and disease intervention.

## Conclusions

In conclusion, our findings have demonstrated that HO binds to FXR in the hepatocytes and upregulates FXR protein level. This, in turn, promotes the transcription and expression of its downstream genes of *SHP* and *CES1*, reduces hepatic lipid deposition and inflammation, and inhibits apoptosis in hepatocytes with lipotoxicity injury. Furthermore, HO exerts its effects through a non-classical mechanism of FXR, inhibiting the protein level of c-CASP8 and directly inhibiting exogenous apoptosis in hepatocytes. The aforementioned effects on inhibition of hepatocyte apoptosis in turn indirectly inhibit HSC activation and exert the anti-NASH fibrosis effects of HO.

## Compliance with ethics requirements

All Institutional and National Guidelines for the care and use of animals (fisheries) were followed.

## Declaration of competing interest

The authors declare that they have no known competing financial interests or personal relationships that could have appeared to influence the work reported in this paper.

## Acknowledgments

This research was supported by the National Nature Science Foundation of China (No. 82170280, U1803125), Beijing Natural Science Foundation (No. 7232093) and Kunming University of Science and Technology & Pu'er People's Hospital Joint Special Project on Medical Research (No. KUST-PE2022006Y). The author would like to express our gratitude to Professor Chang-Tao Jiang of Peking University and Professor Yong-Sheng Chang of Tianjin Medical University for their kindly providing $FXR^{FLOXP}$ mice and Albumin-CRE mice for this study. In addition, the graphical abstract was drawn by Figdraw.

## Appendix A. Supplementary material

Supplementary data to this article can be found online at https://doi.org/10.1016/j.jare.2024.12.016.

## References

[1] Polyzos SA, Chrysavgis L, Vachliotis ID, Chartampilas E, Cholongitas E. Nonalcoholic fatty liver disease and hepatocellular carcinoma: insights in epidemiology, pathogenesis, imaging, prevention and therapy. Semin Cancer Biol 2023:20–35. doi: https://doi.org/10.1016/j.semcancer.2023.04.010.

[2] Younossi ZM, Golabi P, Paik JM, Henry A, Van Dongen C, Henry L. The global epidemiology of nonalcoholic fatty liver disease (NAFLD) and nonalcoholic steatohepatitis (NASH): a systematic review. Hepatology 2023:1335–47. doi: https://doi.org/10.1097/HEP.0000000000000004.

[3] Sheka AC, Adeyi O, Thompson J, Hameed B, Crawford PA, Ikramuddin S. Nonalcoholic steatohepatitis: a review. JAMA-J. Am. Med. Assoc. 2020:1175–83. doi: https://doi.org/10.1001/jama.2020.2298.

[4] Sanyal AJ, Harrison SA, Ratziu V, Abdelmalek MF, Diehl AM, Caldwell S, et al. The natural history of advanced fibrosis due to nonalcoholic steatohepatitis: data from the simtuzumab trials. Hepatology 2019;2019:1913–27. doi: https://doi.org/10.1002/hep.30664.

[5] Angulo P, Kleiner DE, Dam-Larsen S, Adams LA, Bjornsson ES, Charatcharoenwitthaya P, Mills PR, Keach JC, Lafferty HD, Stahler A, Haflidadottir S, Bendtsen F. Liver fibrosis, but no other histologic features, is associated with long-term outcomes of patients with nonalcoholic fatty liver disease. Gastroenterology 2015:389–97. doi: https://doi.org/10.1053/j.gastro.2015.04.043.

[6] Higashi T, Friedman SL, Hoshida Y. Hepatic stellate cells as key target in liver fibrosis. Adv Drug Deliv Rev 2017:27–42. doi: https://doi.org/10.1016/j.addr.2017.05.007.

[7] Schwabe RF, Tabas I, Pajvani UB. Mechanisms of fibrosis development in nonalcoholic steatohepatitis. Gastroenterology 2020:1913–28. doi: https://doi.org/10.1053/j.gastro.2019.11.311.

[8] Feldstein AE, Canbay A, Angulo P, Taniai M, Burgart LJ, Lindor KD, Gores GJ. Hepatocyte apoptosis and fas expression are prominent features of human nonalcoholic steatohepatitis. Gastroenterology 2003:437–43. doi: https://doi.org/10.1016/s0016-5085(03)00907-7.

[9] Schwabe RF, Luedde T. Apoptosis and necroptosis in the liver: a matter of life and death. Nat Rev Gastroenterol Hepatol 2018:738–52. doi: https://doi.org/10.1038/s41575-018-0065-y.

[10] Adorini L, Trauner M. FXR agonists in NASH treatment. J Hepatol 2023:1317–31. doi: https://doi.org/10.1016/j.jhep.2023.07.034.

[11] Xu J, Li Y, Chen WD, Xu Y, Yin L, Ge X, et al. Hepatic carboxylesterase 1 is essential for both normal and farnesoid X receptor-controlled lipid homeostasis. Hepatology 2014;2014:1761–71. doi: https://doi.org/10.1002/hep.26714.

[12] Wang H, Ge C, Zhou J, Guo Y, Cui S, Huang N, Yan T, Cao L, Che Y, Zheng Q, Zheng X, Gonzalez FJ, Wang G, Hao H. Noncanonical farnesoid X receptor signaling inhibits apoptosis and impedes liver fibrosis. EBioMedicine 2018:322–33. doi: https://doi.org/10.1016/j.ebiom.2018.10.028.

[13] Chen Z, He D, Deng J, Zhu J, Mao Q. Chemical composition and antibacterial activity of the essential oil from Agathis dammara (Lamb.) rich fresh leaves. Nat Prod Res 2015:2050–3. doi: https://doi.org/10.1080/14786419.2015.1022544.

[14] Wang A, Yue S, Peng A, Qi R. A review of research progress on Agathis dammara and its application prospects for cardiovascular diseases and fatty liver disease. Mini-Rev Med Chem 2021:670–6. doi: https://doi.org/10.2174/1389557520666201117110834.

[15] Rong Qi, Yingkun Qiu, Ankang Peng, Anyi Wang, Shanshan Yue. Application of *agathis dammara* extract in the preparation of products against non-alcoholic fatty liver disease: China, CN201911255818.7.2021-06-11.

[16] Wang Z, Yu ZW, Zhang Y, Wang WH, Wu XY, Liu SZ, et al. Hinokione: an abietene diterpene with pancreatic beta cells regeneration and hypoglycemic activity, and other derivatives with novel structures from the woods of Agathis dammara. J Nat Med 2024. doi: https://doi.org/10.1007/s11418-024-01816-z.

[17] Tsuchida T, Lee YA, Fujiwara N, Ybanez M, Allen B, Martins S, Fiel MI, Goossens N, Chou HI, Hoshida Y, Friedman SL. A simple diet- and chemical-induced murine NASH model with rapid progression of steatohepatitis, fibrosis and liver cancer. J Hepatol 2018:385–95. doi: https://doi.org/10.1016/j.jhep.2018.03.011.

[18] Machado MV, Cortez-Pinto H. Cell death and nonalcoholic steatohepatitis: where is ballooning relevant? Expert Rev Gastroenterol Hepatol 2011:213–22. doi: https://doi.org/10.1586/egh.11.16.

[19] Canbay A, Taimr P, Torok N, Higuchi H, Friedman S, Gores GJ. Apoptotic body engulfment by a human stellate cell line is profibrogenic. Lab Invest 2003;2003:655–63. doi: https://doi.org/10.1097/01.lab.0000069036.63405.5c.

[20] Hirsova P, Gores GJ. Death Receptor-Mediated Cell Death and Proinflammatory Signaling in Nonalcoholic Steatohepatitis. Cell Mol Gastroenterol Hepatol 2015:17–27. doi: https://doi.org/10.1016/j.jcmgh.2014.11.005.

[21] Zhu C, Kim K, Wang X, Bartolome A, Salomao M, Dongiovanni P, et al. Hepatocyte notch activation induces liver fibrosis in nonalcoholic steatohepatitis. Sci Transl Med 2018. doi: https://doi.org/10.1126/scitranslmed.aat0344.

[22] Kubota N, Kado S, Kano M, Masuoka N, Nagata Y, Kobayashi T, Miyazaki K, Ishikawa F. A high-fat diet and multiple administration of carbon tetrachloride induces liver injury and pathological features associated with non-alcoholic steatohepatitis in mice. Clin Exp Pharmacol Physiol 2013:422–30. doi: https://doi.org/10.1111/1440-1681.12102.

[23] Wang MY, Zhang SS, An MF, Xia YF, Fan MS, Sun ZR, Zhang LJ, Zhao YL, Sheng J, Wang XJ. Neferine ameliorates nonalcoholic steatohepatitis through regulating AMPK pathway. Phytomedicine 2023. doi: https://doi.org/10.1016/j.phymed.2023.154798.

[24] Li N, Zhu C, Fu R, Ma X, Duan Z, Fan D. Ginsenoside Rg5 inhibits lipid accumulation and hepatocyte apoptosis via the Notch1 signaling pathway in NASH mice. Phytomedicine 2024. doi: https://doi.org/10.1016/j.phymed.2023.155287.

[25] Parola M, Pinzani M. Liver fibrosis in NAFLD/NASH: from pathophysiology towards diagnostic and therapeutic strategies. Mol Asp Med 2024. doi: https://doi.org/10.1016/j.mam.2023.101231.

[26] Rahman SR, Roper JA, Grove JI, Aithal GP, Pun KT, Bennett AJ. Integrins as a drug target in liver fibrosis. Liver Int 2022:507–21. doi: https://doi.org/10.1111/liv.15157.

[27] S. Y. Tian, S. M. Chen, C. X. Pan, and Y. Li. FXR: structures, biology, and drug development for NASH and fibrosis diseases. *Acta Pharmacol. Sin.* (2022), 1120-1132. DOI 10.1038/s41401-021-00849-4.

[28] Konigshofer P, Brusilovskaya K, Petrenko O, Hofer BS, Schwabl P, Trauner M, Reiberger T. Nuclear receptors in liver fibrosis. Biochim Biophys Acta-Mol Basis Dis 2021. doi: https://doi.org/10.1016/j.bbadis.2021.166235.

[29] Zhou J, Cui S, He Q, Guo Y, Pan X, Zhang P, et al. SUMOylation inhibitors synergize with FXR agonists in combating liver fibrosis. Nat Commun 2020;240. doi: https://doi.org/10.1038/s41467-019-14138-6.

[30] Carino A, Biagioli M, Marchiano S, Scarpelli P, Zampella A, Limongelli V, Fiorucci S. Disruption of TFGbeta-SMAD3 pathway by the nuclear receptor SHP mediates the antifibrotic activities of BAR704, a novel highly selective FXR ligand. Pharmacol Res 2018:17–31. doi: https://doi.org/10.1016/j.phrs.2018.02.033.

[31] Cui S, Hu H, Chen A, Cui M, Pan X, Zhang P, Wang G, Wang H, Hao H. SIRT1 activation synergizes with FXR agonism in hepatoprotection via governing nucleocytoplasmic shuttling and degradation of FXR. Acta Pharm Sin B 2023:559–76. doi: https://doi.org/10.1016/j.apsb.2022.08.019.

[32] Garcia-Rodriguez JL, Barbier-Torres L, Fernandez-Alvarez S, Gutierrez-de Juan V, Monte MJ, Halilbasic E, Herranz D, Alvarez L, Aspichueta P, Marin JJ, Trauner M, Mato JM, Serrano M, Beraza N, Martinez-Chantar ML. SIRT1 controls liver regeneration by regulating bile acid metabolism through farnesoid X receptor and mammalian target of rapamycin signaling. Hepatology 2014:1972–83. doi: https://doi.org/10.1002/hep.26971.

[33] Quiroga AD, Li L, Trotzmuller M, Nelson R, Proctor SD, Kofeler H, Lehner R. Deficiency of carboxylesterase 1/esterase-x results in obesity, hepatic steatosis, and hyperlipidemia. Hepatology 2012:2188–98. doi: https://doi.org/10.1002/hep.25961.

[34] C. Gan, J. Wang, A. Martinez-Chavez, M. Hillebrand, N. de Vries, J. Beukers, E. Wagenaar, Y. Wang, M. C. Lebre, H. Rosing, S. Klarenbeek, R. B. Ali, C. Pritchard, I. Huijbers, J. H. Beijnen, and A. H. Schinkel. Carboxylesterase 1 family knockout alters drug disposition and lipid metabolism. *Acta Pharm. Sin. B* (2023), 618-631. 10.1016/j.apsb.2022.10.017.

[35] Liu J, Yao B, Gao L, Zhang Y, Huang S, Wang X. Emerging role of carboxylesterases in nonalcoholic fatty liver disease. Biochem Pharmacol 2022. doi: https://doi.org/10.1016/j.bcp.2022.115250.

[36] Harrison SA, Goodman Z, Jabbar A, Vemulapalli R, Younes ZH, Freilich B, Sheikh MY, Schattenberg JM, Kayali Z, Zivony A, Sheikh A, Garcia-Samaniego J, Satapathy SK, Therapondos G, Mena E, Schuppan D, Robinson J, Chan JL, Hagerty DT, Sanyal AJ. A randomized, placebo-controlled trial of emricasan in patients with NASH and F1–F3 fibrosis. J Hepatol 2020:816–27. doi: https://doi.org/10.1016/j.jhep.2019.11.024.

[37] Harrison SA, Wong VW, Okanoue T, Bzowej N, Vuppalanchi R, Younes Z, Kohli A, Sarin S, Caldwell SH, Alkhouri N, Shiffman ML, Camargo M, Li G, Kersey K, Jia C, Zhu Y, Djedjos CS, Subramanian GM, Myers RP, Gunn N, Sheikh A, Anstee QM, Romero-Gomez M, Trauner M, Goodman Z, Lawitz EJ, Younossi Z. Selonsertib for patients with bridging fibrosis or compensated cirrhosis due to NASH: results from randomized phase III STELLAR trials. J Hepatol 2020:26–39. doi: https://doi.org/10.1016/j.jhep.2020.02.027.

[38] Hindson J. Obeticholic acid for the treatment of NASH. Nat Rev Gastroenterol Hepatol 2020;66. doi: https://doi.org/10.1038/s41575-020-0264-1.

[39] Jiang M, Huang C, Wu Q, Su Y, Wang X, Xuan Z, Wang Y, Xu F, Ge C. Sini San ameliorates CCl4-induced liver fibrosis in mice by inhibiting AKT-mediated hepatocyte apoptosis. J Ethnopharmacol 2023. doi: https://doi.org/10.1016/j.jep.2022.115965.